Science of Remote Sensing 5 (2022) 100057

Contents lists available at ScienceDirect

Science of Remote Sensing

journal homepage: www.sciencedirect.com/journal/science-of-remote-sensing

A new procedure for evaluating light-to-moderate earthquake location based on InSAR data and forward modeling tested on Mediterranean area

M. Polcari *, S. Atzori, I. Munafò

Istituto Nazionale di Geofisica e Vulcanologia, Italy

ARTICLE INFO

Keywords:
Moment tensor solution
Sentinel-1
InSAR data
Mediterranean area
Light-to-moderate earthquake

ABSTRACT

We propose a procedure based on remote sensing Sentinel-1 InSAR data aiming at evaluating the variability of the moment tensor solutions provided by different agencies in case of light-to-moderate earthquake. We model the expected coseismic ground deformations from the available moment tensor solutions and compare them with the real ones retrieved with the InSAR data. Any differences between location and intensity of simulated and estimated seismic-induced deformation fields allow indirectly evaluating the variability of the solutions in terms of epicenter locations and kinematics of the causative faults.

We applied this investigation method to several light ($4<M_w<4.9$) to moderate ($5<M_w<5.9$) earthquakes occurred along the Mediterranean area since the launch of the Sentinel-1A mission in 2014. The selected seismic events cover all the faulting mechanisms and are characterized by different estimated magnitudes and depths thus offering a synoptic view of the performance of the procedure in several cases. Thanks to the global coverage and the unprecedented revisit time of Sentinel-1 acquisitions, the proposed procedure can be easily extended to any seismic event occurred inland worldwide.

1. Introduction

The precise location and the kinematics of the rupture during an earthquake is one of the most important issues for supporting tectonic studies and seismic hazard assessment purposes [Dziewonski et al., 1981; Lentas et al., 2019; Karasözen and Karasözen, 2020]. However, achieving accurate and bias-free earthquake locations and kinematics is often challenging due to unfavorable configuration of the seismic networks and the uncertainties of the techniques, especially when the magnitude of the event ranges from minor (Mw 3–3.9) to moderate (Mw 5–5.9). Several providers, such as USGS, the Global CMT project, INGV with TDMT [Scognamiglio et al., 2006] and RCMT [Pondrelli, 2002] techniques, GFZ, etc. provide the coordinates of the epicenter and the moment tensor starting from few minutes after an earthquake, but sometimes the solutions show significant differences thus revealing a great variability in the estimation of such parameters .

In this context, the development of remote sensing Synthetic Aperture Radar (SAR) sensors, observing and continuously acquiring images of the Earth's surface, marked a turning point. Several missions and data processing techniques, with particular focus on SAR Interferometry (InSAR) [Massonet et al., 1993], have rapidly grown since the ERS-1 mission of the European Space Agency (ESA) in 1992. InSAR data proved to be an useful tool in seismology to detect the real ground surface deformation induced by a seismic event and thus supporting the overall rupture location and fault geometry constraining. Nowadays, InSAR data are largely applied in the study of seismic events to improve the knowledge of the seismic sources and the slip distributions through the modeling of geodetic data [Wright et al., 2003; Schmidt et al., 2006; Atzori et al., 2009; Kobayashi et al., 2012; Cheloni et al., 2017; Wang et al., 2018; Wang et al., 2019; Svikgas et al., 2021].

However, in case of Mw < 6 earthquakes, depending on depth and magnitude, the induced surface deformation can be in the order of a few centimeters or also subcentimetric, i.e. close to the detectability limits of InSAR data [Massonet and Feigl, 1998]. At this scale, it could be very difficult to discriminate the deformation signal from small atmospheric artifacts or noise without integrating other information sources.

We therefore propose, in this work, a method of investigation with a twofold aim: i) investigating the variability of the moment tensor solutions provided by different agencies in case of light-to-moderate earthquakes; ii) supporting the choice of the best InSAR data according to the properties of the seismic event.

To this purpose we exploit the moment tensor solutions provided by

* Corresponding author.
E-mail address: marco.polcari@ingv.it (M. Polcari).

https://doi.org/10.1016/j.srs.2022.100057
Received 16 February 2022; Received in revised form 14 April 2022; Accepted 9 May 2022
Available online 13 May 2022

Table 1
List of the agencies whose solutions have been used in this work.

Agency	Acronym	Nation
United States Geological Survey	USGS	USA
Istituto Nazionale di Geofisica e Vulcanologia	INGV	Italy
German Research Center for Geosciences	GFZ	Germany
Global Centroid Moment Tensor	GCMT	USA
National Observatory of Athens	NOA	Greece
Aristotle University of Thessaloniki	AUTH	Greece
Institut de Physique du Globe de Paris	IPGP	France
Kandilli Observatory and Earthquake Research Institute	KOERI	Turkey
Earthquake Research Directorate	ERD	Turkey

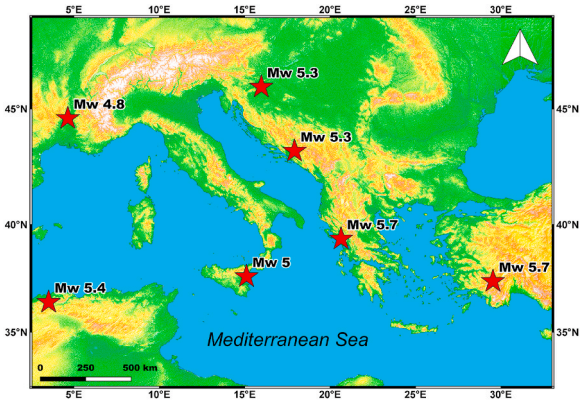

Fig. 1. Location of the seismic events analyzed in this work. Location and magnitude are from USGS.

several agencies (Table 1) for some selected earthquakes to simulate the seismic-induced ground displacement; in addition to the strike, dip and rake angles and the event location/depth, we use the Wells and Coppersmith (1994) rules [Wells and Coppersmith, 1994] to derive length and width from the scalar moment, getting the whole parameters of a finite source. The latter is then used as input to the analytical equation for a shear dislocation in an elastic half-space [Okada, 1985] to derive the surface displacement map. Then, based on the simulated displacement field we choose and process the InSAR data to get the real coseismic ground deformation thus evaluating the variability of solutions estimated by the agencies.

We applied this investigation method to several light (Mw 4–4.9) to moderate (Mw 5–5.9) earthquakes that occurred along the Mediterranean area in the last few years (Fig. 1). Our analysis is based on the application of SAR data provided by Sentinel-1 (S1) mission of the European Space Agency (ESA) Copernicus project, since it provides a global coverage of the Earth's surface with an unprecedented revisit time of 6 days and all the acquisitions are easily accessible free of charge. Such features allow to study any seismic event occurring worldwide in near-real time conditions and then to easily extend the proposed procedure to a global scale.

2. Case studies

We selected 7 light-to-moderate earthquakes occurred from 2016 to 2020 in several countries, i.e. Algeria, Bosnia-Herzegovina, Croatia, France, Greece, Italy and Turkey, along the Mediterranean region (Table 2). Our survey is based on the following criteria:

1) Starting point in 2014;
2) Minimum magnitude equal to 4.5;
3) Maximum magnitude equal to 5.9;
4) Discarding the events with foreshocks and aftershocks with magnitude comparable with the mainshock.

Table 2
Overview on the seismic events chosen for this study.

Country	Date	Agency	Latitude (°)	Longitude (°)	Moment Magnitude (M_w)	Depth (Km)
Algeria	28-05-2016	USGS	36.43	3.51	5.4	11.5
		GFZ	36.40	3.49	5.2	10
		INGV	36.30	3.40	5.3	10
		RCMT				
Italy	26-12-2018	USGS	37.63	15.10	5	1
		INGV	37.64	15.12	4.9	3
		TDMT				
		INGV	37.60	15.2	5	8
		RCMT				
Turkey	20-03-2019	USGS	37.40	29.53	5.7	8
		GFZ	37.46	29.48	5.7	16
		GCMT	37.37	29.38	5.7	12
		KOERI	37.45	29.43	5.5	12
		ERD	37.44	29.43	5.7	12.1
		IPGP	37.40	29.60	5.7	7
France	11-11-2019	USGS	44.61	4.63	4.8	10
		GFZ	44.59	4.65	4.9	13
		INGV	44.50	4.50	4.9	10
		RCMT				
Bosnia Herz.	26-11-2019	USGS	43.22	17.91	5.3	10
		INGV	43.16	17.98	5.1	16
		TDMT				
		GFZ	43.20	17.98	5.3	23
		INGV	43.21	18.08	5.4	32
		RCMT				
Greece	21-03-2020	USGS	39.35	20.63	5.7	10
		GFZ	39.36	20.61	5.7	16
		NOA	39.32	20.52	5.5	7.9
		GCMT	39.16	20.56	5.7	13.6
		AUTH	39.30	20.62	5.7	7
		IPGP	39.35	20.56	5.8	10
		INGV	39.20	20.60	5.7	14
		RCMT				
Croatia	22-03-2020	USGS	45.90	15.97	5.1	10
		INGV	45.85	15.95	5.3	6
		TDMT				
		GFZ	45.89	16.00	5.3	10
		INGV	45.80	16.10	5.4	11
		RCMT				

The starting point corresponds to the launch of the first C-band S1 mission of ESA, in April 2014, followed by S1–B on april 2016. As stated above, the synergistic use of both missions allows to retrieve a global coverage with revisit time of 6 days which are important requirements for the application of the procedure. The second and third criteria define the investigation scale which is focused on light to moderate earthquakes. Indeed, the locations of stronger seismic events (Mw > 6) are clearly easier to constrain due to the significant intensity of the seismic waves. On the other hand, the lower bound is fixed to 4.5 since there is very little evidence of surface deformation induced by Mw < 4.5 seismic event [Albano et al., 2018]. Finally, the fourth criteria aim to maximize the probability of detection of the seismic-induced surface deformation by InSAR data since aftershock or foreshock signals could mask or affect the mainshock deformation.

Depending on the agency, not only the location but also the magnitude and the seismic source parameters can vary. The studied seismic events are characterized by an M_w magnitude ranging from 4.8 to 4.9, for the France earthquake, to 5.7–5.8, in the case of both Greece and Turkey earthquakes according to the different solutions. The estimated source depth, one of the most important parameters for the propagation of the deformation on the surface, is in the order of about 10–20 km for most cases, with great discrepancies between solutions in the case of the Greece earthquake. The only exception is represented by the Italy earthquake where both USGS and INGV TDMT solutions are quite surficial (1-3 Km) and consistent with volcanic induced earthquakes being caused by the Mt. Etna eruption on December 24th, 2018 [Bonforte et al., 2019; De Novellis et al., 2019].

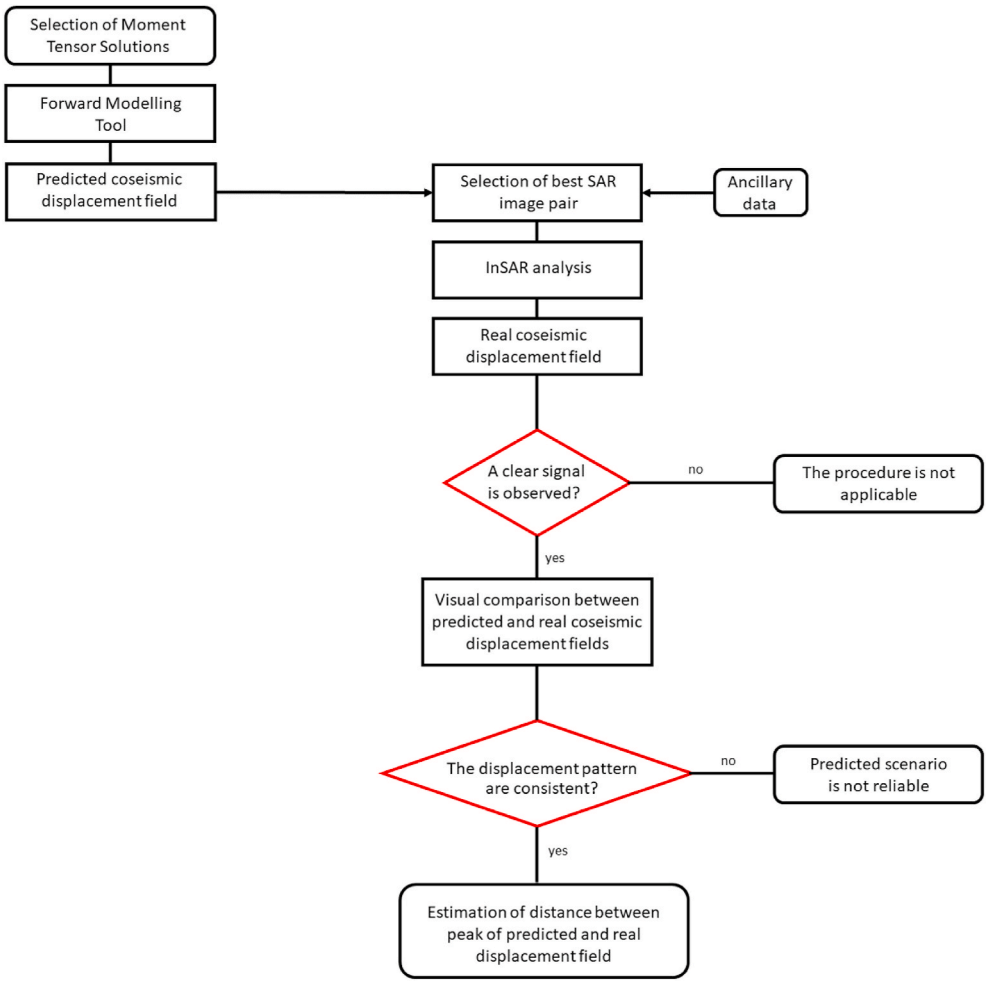

Fig. 2. Flowchart of the proposed procedure.

3. InSAR data

InSAR data used in this work consist of pairs of S1 SAR images covering the seismic events in Table 1. The revisit time of the pairs is 6 days according to the S1-A/B missions apart from the Algeria case study since SAR data from S1–B missions were still not available in May–June 2016. The data were processed with the standard InSAR approach. We multi-looked the images by 8 × 2 factors thus retrieving an about 30 × 30 m pixel size which is the same as the 30 m Digital Elevation Model (DEM) of the Shuttle Radar Topography Mission (SRTM) used for removing the topography from the SAR interferometric phase. The retrieved interferograms were then filtered [Goldstein and Werner, 1998] unwrapped [Costantini, 1998] and refined by in-house scripts developed in Linux Bash Shell scripting. Displacement maps for all the seismic events have been then geocoded and represented in QGIS environment.

4. Methodology/procedure

The flowchart of the procedure is shown in Fig. 2.

First, we perform an extensive research of the moment tensor solutions provided by the different agencies. All the solutions for any earthquake are collected in a catalog by the European Mediterranean Seismological Centre (EMSC) and made available online at the following link https://www.emsc-csem.org/Earthquake/tensors.php. Therefore, the source parameters of each solution, i.e. latitude, longitude, seismic moment, depth and rupture direction (strike, dip and rake angles) are used to run a forward modelling to predict the ground displacement. This is carried out by firstly defining the length and width of a finite source, using the scaling factors of Wells and Coppersmith (1994), keeping the center of the fault at the point-source location of the focal mechanism. In some cases, the InSAR fringe pattern allows discriminating between the real and the auxiliary fault; for events with depth greater than three-four times the fault dimension, the point-source approximation is valid and the predicted surface displacements are essentially the same for both nodal planes. Based on Sentinel-1 ascending and descending geometry of view, all the retrieved maps are then projected into the satellite Line-of-Sight (LoS) for both orbits. This allows us to have a preliminary overview on the expected seismic-induced ground deformation. Moreover, it also provides a sort of guideline for the choice of the most suitable SAR image pair, i.e. the pair acquired along ascending or descending track, to process. Indeed, depending on the faulting mechanism and the orientation of the causative fault with respect to the satellite geometry of view, possible displacement fields could be better or only detected by one of the two orbiting directions, i.e. ascending or descending. This is mainly due to any horizontal deformation components which produce opposite displacement values along ascending and descending track. Ancillary data concerning the knowledge of the geomorphology and the faults system in the area hit by the seismic event can also support this step. Once chosen the best SAR images pair, InSAR data processing is performed and any real coseismic ground deformation is retrieved. In the case of absence of any clear signal ascribable to the seismic event, the procedure ends since there is no surface evidence to be compared. Otherwise, based on a simple visual inspection, the consistency in terms of spatial extent and shape between simulated and real coseismic

deformation pattern has to be evaluated. If there is a strong disagreement between the two data, the procedure ends because our scenarios based on moment tensors are not able to depict the real deformation pattern. This means that, due to several reasons, some parameters of the causative fault estimated by the agencies could be not precise and the predicted scenario could be not completely reliable. Instead, in case of good agreement, the kinematics of the fault estimated by the agencies and the subsequent predicted scenario can be considered very close to the real and additional analysis to estimate the distance between the peak of the simulated and real displacement pattern are needed to further evaluate the precision of the solution.

5. Results

For sake of simplicity, we show the analytical procedure using only one focal plane. Indeed, for inverse and normal faulting mechanisms the seismic-induced ground displacements simulated from moment tensor solutions is approximately the same for both nodal planes, provided that the rupture does not reach the surface, as instead often happens with strike-slip faulting mechanism, i.e. for Bosnia-Herzegovina and Italy case studies. However, for Bosnia-Herzegovina earthquake there is no evidence of ground deformation for both focal planes whereas for Italy earthquake we chose the one consistent with the known faults system of the area [Azzaro et al., 2001; Neri et al., 2004]. Particular care is required for the choice of the simulated ground displacements representation scale that we set between −1/+1 cm since, when considering InSAR data, an entire interferometric fringe represents a LoS displacement of half wavelength, meaning about 2.8 cm for the C-band S1 data (λ∼5.6 cm). Therefore, the InSAR detectability threshold can be empirically considered about a quarter of wavelength, i.e. at least half interferometric fringe has to be observed (∼1.4 cm), below which the signal has a comparable intensity of the typical InSAR correlated noise mainly due to atmospheric artifacts. Moreover, in case of light to moderate earthquakes, it is reasonable to expect ground deformation in the order of few centimeters or also subcentimeter.

5.1. Algeria

In the case of the Algeria earthquake in 2016, three moment tensor solutions are available provided by USGS, GFZ and INGV RCMT. Therefore, based on these solutions, we estimate the simulated LoS coseismic displacement projected along both ascending and descending LOS by forward modelling tool (Fig. 3).

The coseismic displacement modelled by USGS, GFZ and INGV RCMT moment tensor solutions show for all of them a greater impact when projected along ascending track with respect to descending one. It is clearly observed for USGS and INGV RCMT (Fig. 3, panel A,B,E,F), where almost 1 cm of deformation is estimated along ascending orbit but also for GFZ solution although the estimated values are subcentimetric.

Such results lead to the selection of ascending S1 images for the InSAR data processing since, given the available solutions for this event, the probability to detect a coseismic signal by InSAR data is maximized

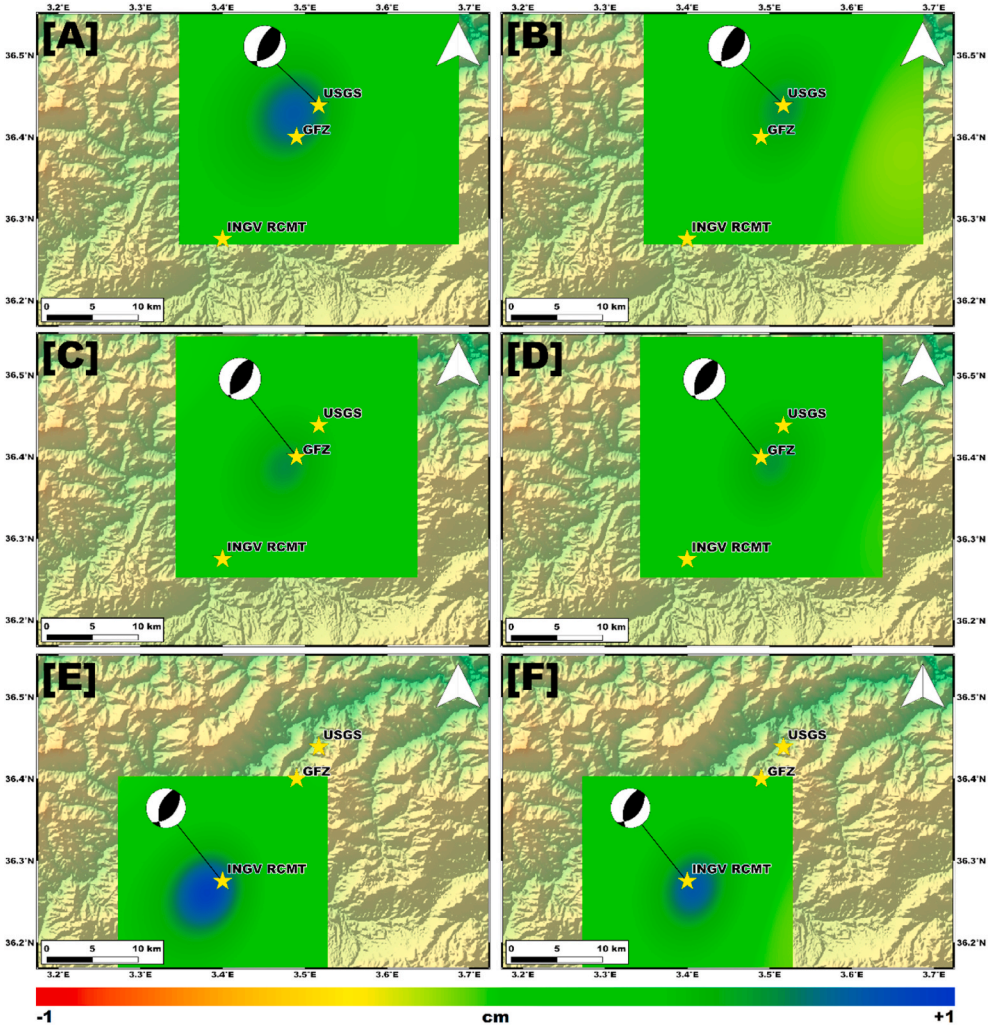

Fig. 3. LoS coseismic ground displacement of the 2016 Algeria earthquake simulated from USGS, GFZ and INGV RCMT moment tensor solutions. USGS solution projected along S1 ascending (A) and descending (B) track. GFZ solution projected along ascending (C) and descending (D) track. INGV RCMT solution projected along ascending (E) and descending (F) track. The yellow stars indicate the epicenters estimated. The background image is the SRTM DEM. (For interpretation of the references to colour in this figure legend, the reader is referred to the Web version of this article.)

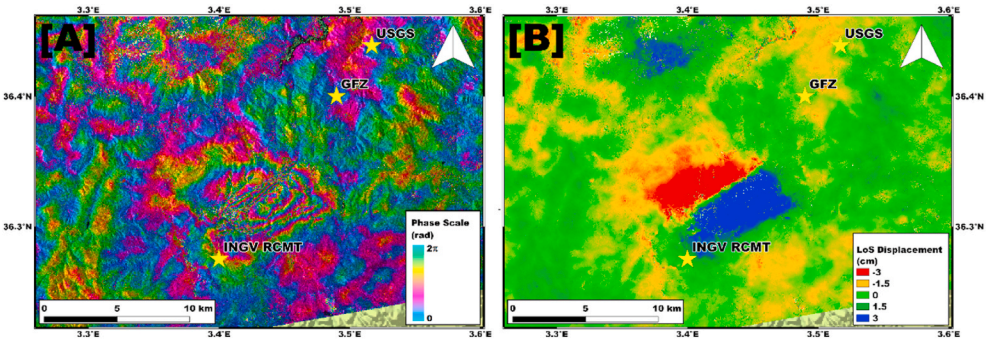

Fig. 4. S1 wrapped interferogram (A) and Displacement map (B) related to the 2016 Algeria earthquake.

along ascending track than descending one.

Then, in the case of the Algeria earthquake occurred on May 28th, 2016, we selected two S1-A images acquired on May 24th and June 6th, 2016. The results of InSAR data processing is shown in Fig. 4.

InSAR data evidence a complex coseismic displacement pattern far about 12 Km and 8 Km from the USGS and GFZ epicenters, whereas the INGV RCMT is the closest to the real deformation pattern (about 6 Km). Moreover, InSAR outcomes seem to reveal a surface rupture with deformation value ranging from about −3 to +3 cm along the two sides of the fault, likely involving a significant horizontal or a subsidence component during the event. This is inconsistent with the quasi-pure reverse faulting mechanism estimated by USGS, GFZ and INGV RCMT solutions.

Therefore, for the 2016 Algeria earthquake the predicted scenarios seem not to be representative both in terms of epicenter location and fault kinematics of the real faulting process occurred during the seismic event.

5.2. *Italy*

This seismic event occurred on December 26th, 2018, triggered by an intense eruptive phase of Mt Etna volcano starting on December 23rd. As

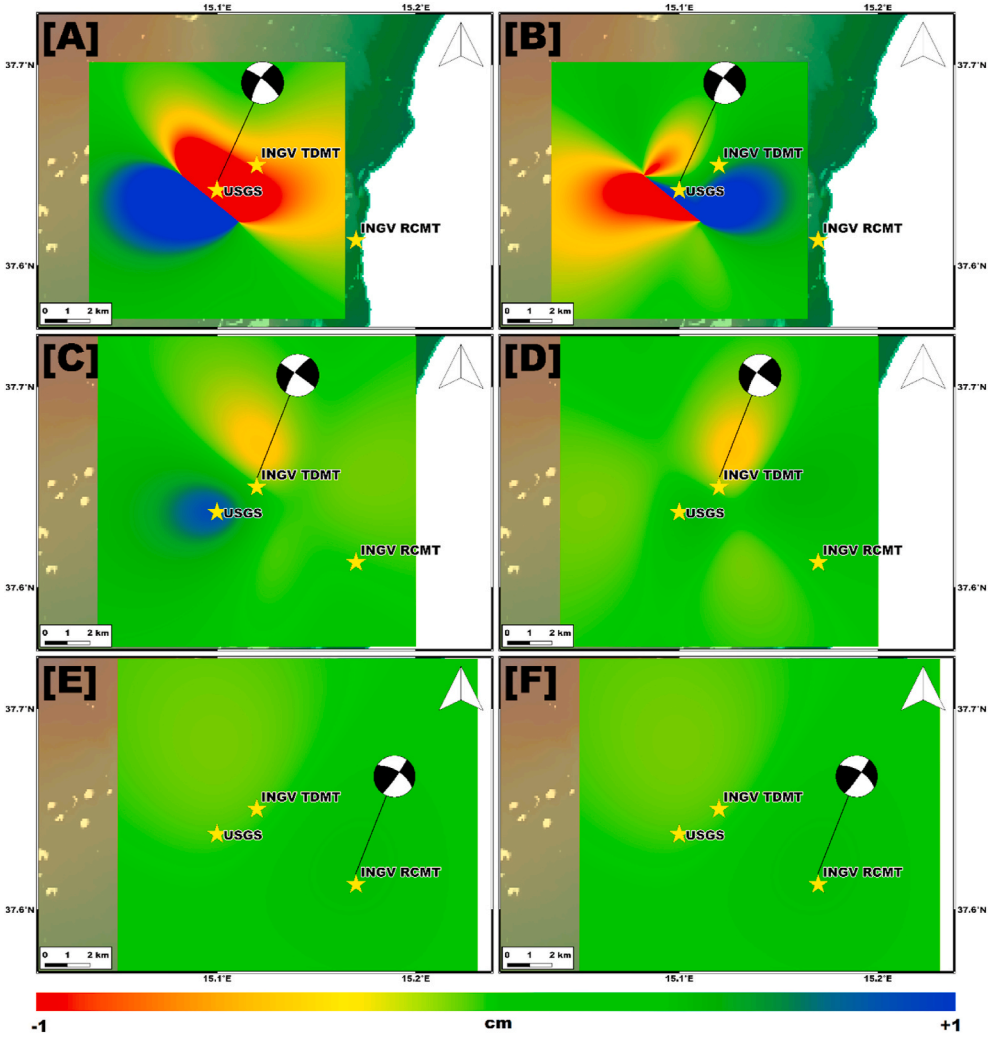

Fig. 5. LoS coseismic ground displacement of the 2018 Italy earthquake simulated from USGS, INGV TDMT and RCMT moment tensor solutions. USGS solution projected along S1 ascending (A) and descending (B) track. INGV TDMT solution projected along ascending (C) and descending (D) track. INGV RCMT solution projected along ascending (E) and descending (F) track. The yellow stars indicate the epicenters estimated. The background image is the SRTM DEM. (For interpretation of the references to colour in this figure legend, the reader is referred to the Web version of this article.)

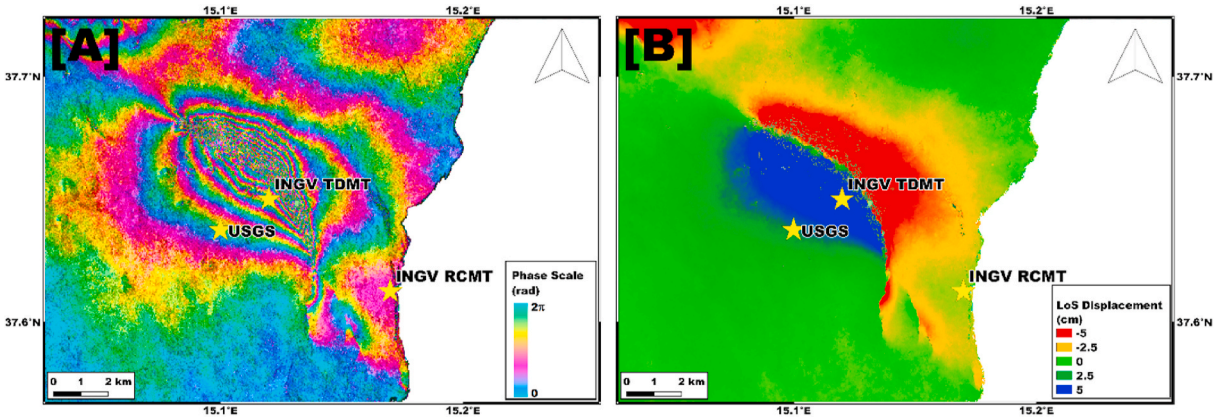

Fig. 6. S1 wrapped interferogram (A) and Displacement map (B) related to the 2018 Italy earthquake.

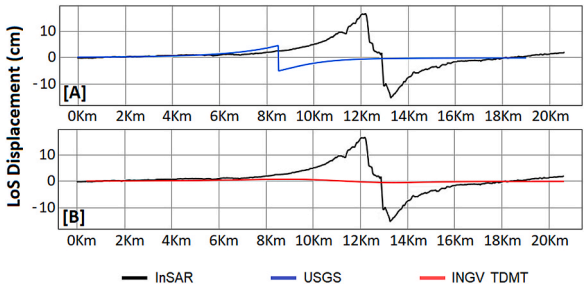

Fig. 7. Comparison between LoS displacement retrieved by InSAR data and derived from USGS [A] and INGV TDMT [B] solutions along transepts crossing the related peak deformation values in the case of 2018 Italy earthquake.

shown in several works [Bonforte et al., 2019; De Novellis et al., 2019], it nucleated along the Fiandaca fault, which is a NW-SE right lateral trending active structure .

Consistently, the moment tensor solutions available for this event, provided by USGS, INGV TDMT and RCMT, show a mainly strike-slip faulting mechanism. Then, based on the seismotectonic settings of the area, we selected the focal plane accordingly. The coseismic displacements simulated from USGS and INGV TDMT solutions show a clear pattern along ascending orbit whereas the one simulated from INGV RCMT solution is basically undetectable for both orbits (see Fig. 5). Such results lead to the selection of the ascending SAR data acquired on December 22nd and 28th. InSAR results show a complex pattern consistent with a mainly strike-slip faulting mechanism characterized by several fringes peaking at about +-10 cm (see Fig. 6). The features of this pattern are in agreement with the ones shown in the predicted scenarios from USGS and INGV TDMT solutions, then, we evaluate the distance between deformation peaks of predicted and real scenarios. Both USGS and INGV TDMT derived results are close to the real scenario being shifted about 3.5 Km and 1.5 Km from the InSAR deformation pattern, respectively. However, they underestimate the real deformation, especially the one from INGV TDMT whose deformation peak is indeed almost undetectable from visual inspection of Fig. 7.

5.3. Turkey

In this case, six moment tensor solutions are available provided by

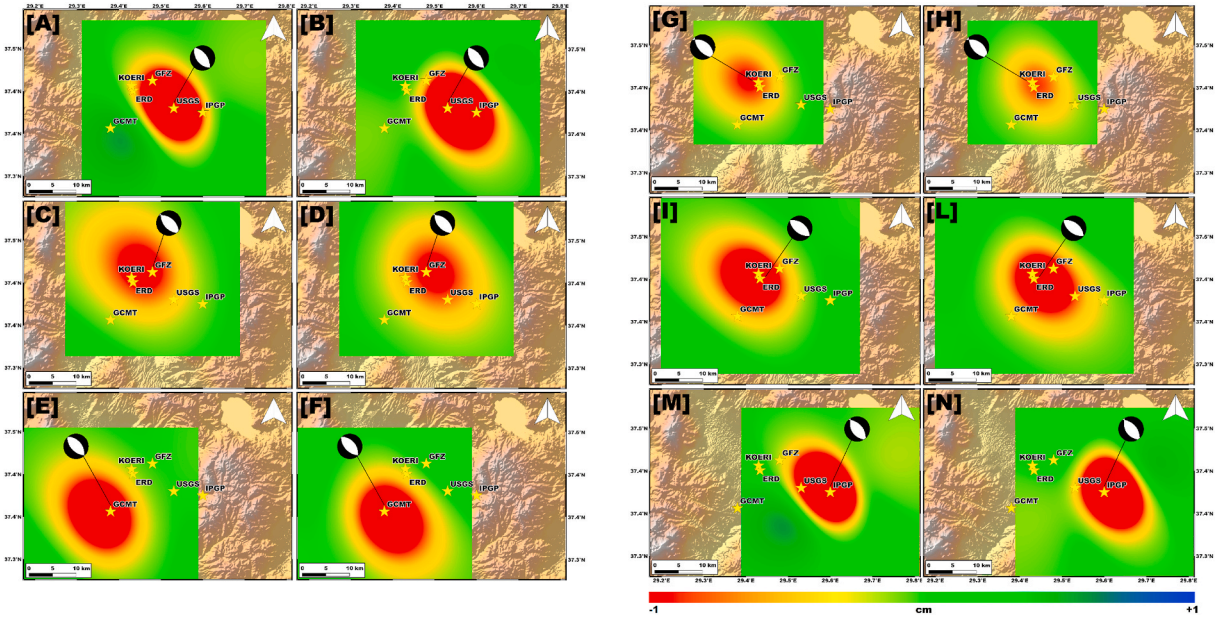

Fig. 8. LoS coseismic ground displacement of the 2019 Turkey earthquake simulated from USGS (A,B), GFZ (C,D), GCMT (E,F), KOERI (G,H) ERD (I,L) and IPGP (M, N) moment tensor solutions and projected along S1 ascending (left column) and descending (right column) track. The yellow stars indicate the epicenters. The background image is the SRTM DEM. (For interpretation of the references to colour in this figure legend, the reader is referred to the Web version of this article.)

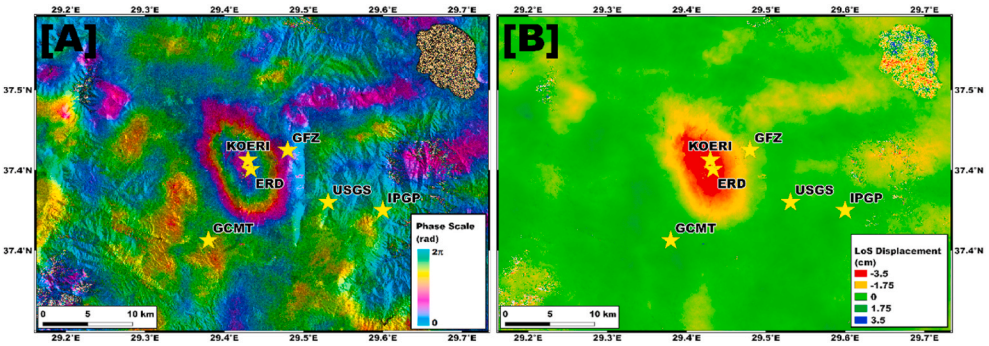

Fig. 9. S1 wrapped interferogram (A) and Displacement map (B) related to the 2019 Turkey earthquake.

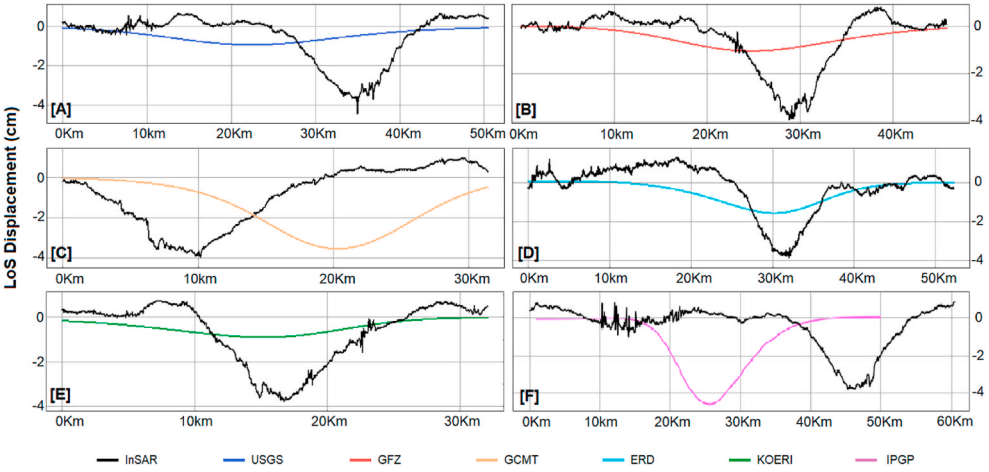

Fig. 10. Comparison between LoS displacement retrieved by InSAR data and derived from USGS [A], GFZ [B], GCMT [C], ERD [D], KOERI [E] and IPGP [F] solutions along transepts crossing the related peak deformation values in the case of 2019 Turkey earthquake.

USGS, GFZ, GCMT, ERD, KOERI and IPGP. LoS Simulated coseismic displacements show almost the same pattern when projected along S1 ascending and descending track both in spatial extent and in magnitude for all the solutions (Fig. 8). This theoretically means that there is no favoured geometry of view and it is possible to indifferently choose one of the two tracks. Here we selected the S1 ascending images pair acquired on March 17th and 23rd and the results of InSAR data processing is shown in Fig. 9.

InSAR-derived coseismic displacement is consistent with the mainly normal faulting mechanism estimated by all the available solutions showing a LoS deformation peaking at about −3.5/-4 cm. In addition, the shape and the spatial extent of all the simulated and the real seismic-induced ground deformation patterns are in good agreement thus requiring additional analysis to evaluate the reliability of the solutions.

In particular, a profile analysis along transepts crossing the peak-to-peak deformation values show how USGS, GCMT, GFZ and IPGP solutions are the most inaccurate in terms of position as observed by a simple visual inspection of Fig. 10. Such solutions are characterized by a peak-to-peak distance from the InSAR estimated coseismic displacement of about 9 Km, 8 Km, 4 Km and 20 Km, respectively.

On the other hand, ERD and KOERI solutions seem to better reproduce spatial extent and position but the latter significantly underestimate the real deformation. Also for USGS, GFZ and ERD solutions there is a misfit of about 1.5/2 cm between the peak deformation values estimated by InSAR data and the ones modelled by the moment tensor solutions. Instead, although shifted about 8 km south-west, and 20 Km south-east, the GCMT and IPGP solutions are the only reproducing the magnitude of the coseismic deformation induced by the event.

5.4. France

Three moment tensor solutions are available for this event, provided by USGS, GFZ and INGV RCMT respectively.

All solutions indicate an almost pure reverse faulting mechanism but the simulated LoS coseismic displacements do not show any ground deformation pattern (Fig. 11). The same is observed for both tracks then no deformations detectable within the limit of accuracy of the technique should be expected by InSAR data.

Since not favoured geometry is shown, to perform InSAR analysis we choose the S1 ascending pair, acquired on November 6th and 12th, 2019. The results are shown in Fig. 12. Despite the light magnitude of the event (<5 for all agencies), we find an entire interferometric fringes, i.e. 2.8 cm LoS deformation, along each of the two sides of an approximately SW-NE fault rupture. Such InSAR deformation pattern indicates a complex rupture process during the earthquake with evidence on the surface likely involving both vertical and horizontal displacement. Moreover, the clear signal observed in InSAR data likely indicates a shallower seismic source (Cornou et al., 2021; Causse et al., 2021) than the one estimated by the agencies, at more than 10 Km depth. Therefore, as for the Algeria case study, in this case the provided solutions seem not to well reproduce the real rupture process.

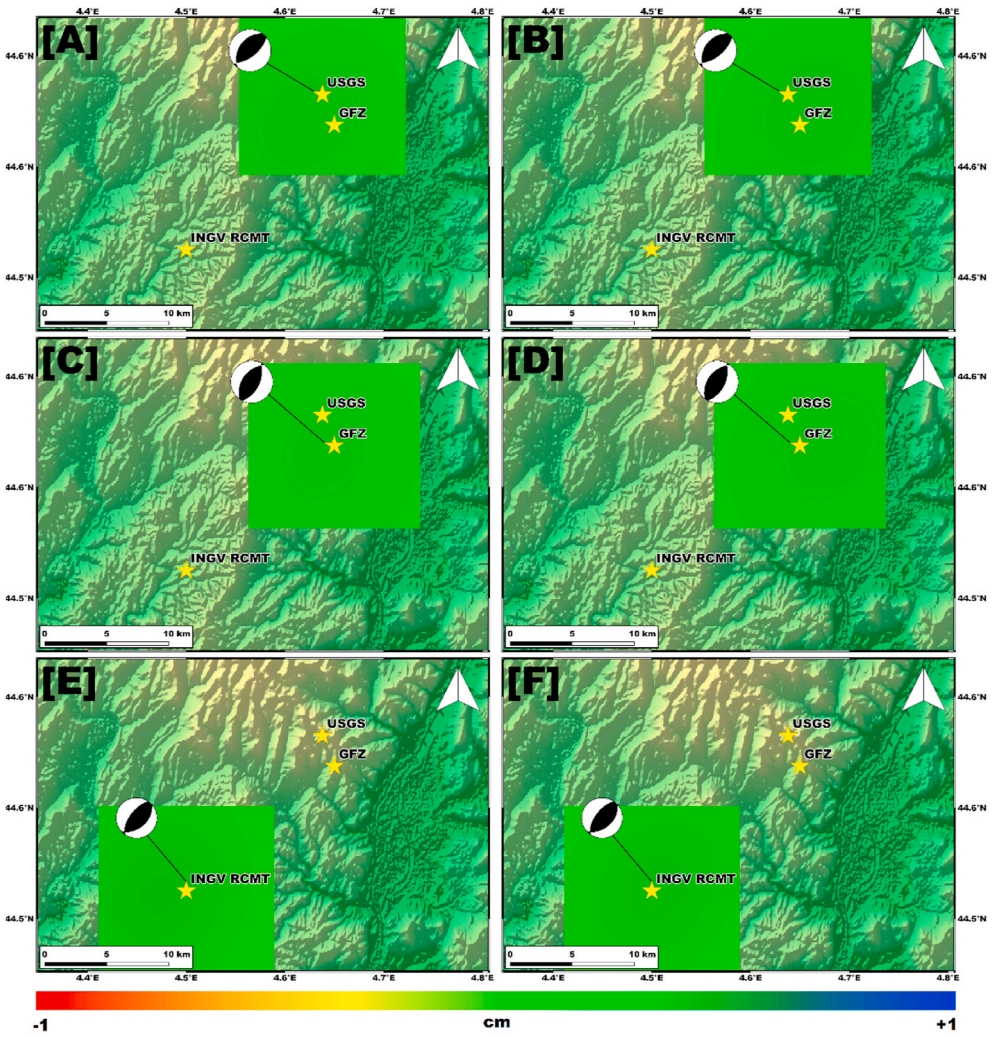

Fig. 11. LoS coseismic ground displacement of the 2019 France earthquake simulated from USGS (A,B) and GFZ (C,D) moment tensor solutions and projected along S1 ascending (left column) and descending (right column) track. The yellow stars indicate the epicenters estimated by USGS and GFZ, IPGP and OCA. The background image is the SRTM DEM. (For interpretation of the references to colour in this figure legend, the reader is referred to the Web version of this article.)

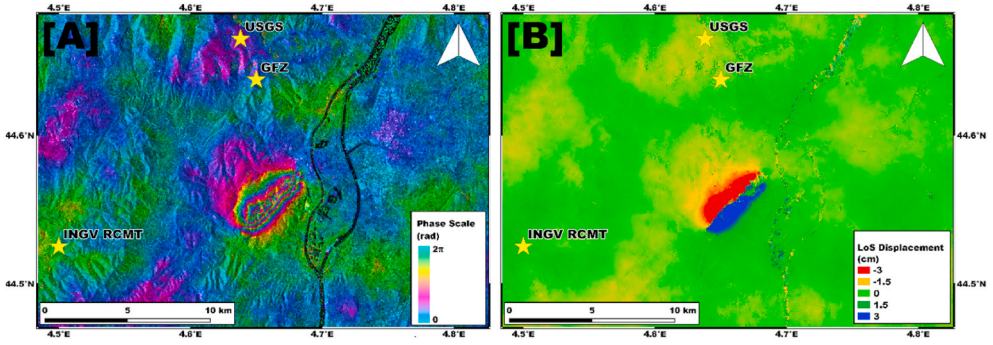

Fig. 12. S1 Wrapped interferogram (A) and Displacement map (B) related to the 2019 France earthquake.

5.5. *Bosnia-Herzegovina*

Four moment tensor solutions are available from USGS, GFZ and INGV TDMT and RCMT, all showing a strike-slip faulting mechanism (Fig. 13). None of these show any LoS ground deformation along both tracks probably due to the estimated depth of the event, spanning from 10 Km to 32 Km (see Table 2).

Therefore, we try to analyse both ascending and descending S1 SAR images obtaining similar results. Here we show the outcomes from the S1 descending data acquired on November 24th and 30th, 2019, respectively (Fig. 14).

Unfortunately, also InSAR data do not highlight any ground deformation pattern. In the proximity of the USGS epicenter is detected a very small signal but it is represented by less than half interferometric fringe and thus cannot be discriminated from any atmospheric artifact. Then, this is a case where the proposed method of investigation does not add

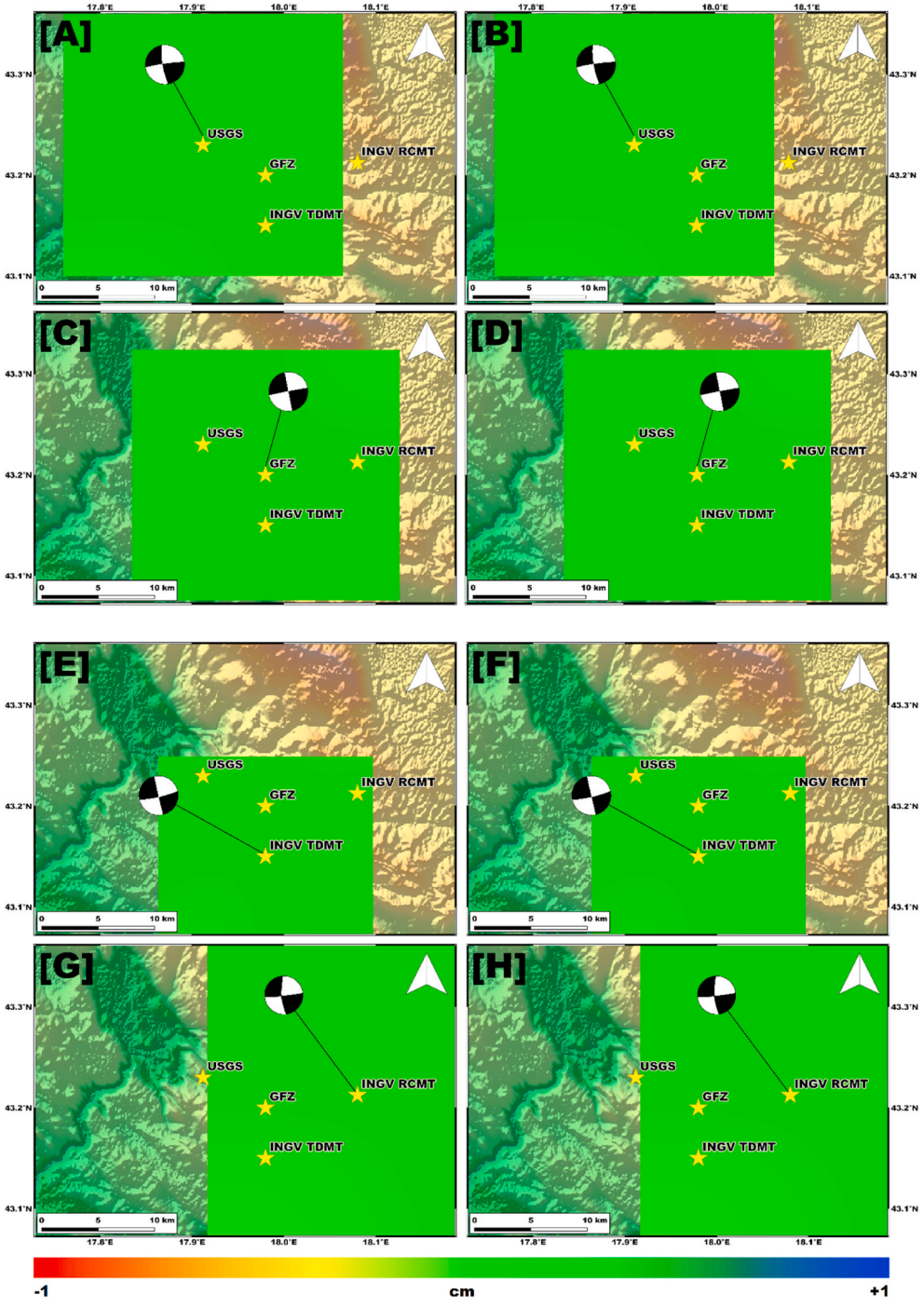

Fig. 13. LoS coseismic ground displacement of the 2019 Bosnia-Herzegovina earthquake simulated from USGS (A,B), GFZ (C,D), INGV TDMT (E,F) and RCMT (G,H) moment tensor solutions and projected along S1 ascending (left column) and descending (right column) track. The yellow stars indicate the epicenters estimated by the agencies. The background image is the SRTM DEM. (For interpretation of the references to colour in this figure legend, the reader is referred to the Web version of this article.)

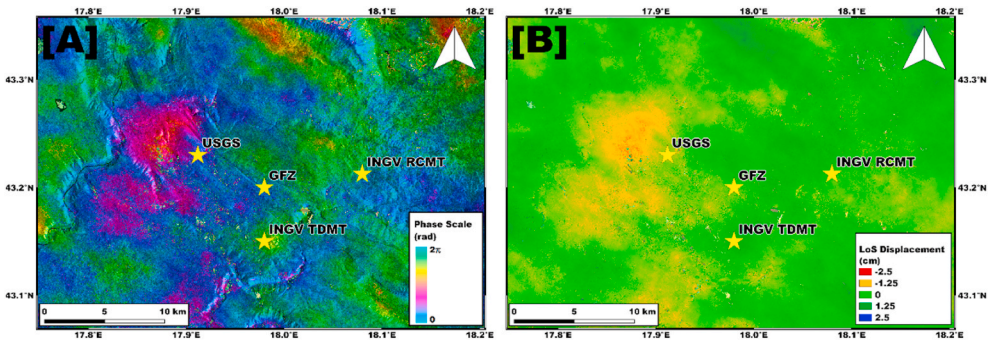

Fig. 14. S1 Wrapped interferogram (A) and Displacement map (B) related to the 2019 Bosnia-Herzegovina earthquake.

useful information and the evaluation of the variability of the solution provided by the agencies both in terms of kinematics and epicenter location is not allowed.

5.6. Greece

Such event occurred on March 20th, 2020 in Epirus region (north-western Greece) in a non particularly seismically active area. This is the earthquake with the greatest number of available moment tensor solutions with seven solutions provided by USGS, GFZ, GCMT, INGV RCMT, IPGP, AUTH and NOA.

All the simulated solutions show a reverse faulting mechanism and, as for the Turkey earthquake, there is no favoured satellite geometry (Fig. 15) then we chose the descending one. We selected S1 descending data acquired on March 19th and 25th to isolate the mainshock and the results of InSAR processing are shown in Fig. 16. InSAR wrapped interferogram highlight almost an entire interferometric fringe (Fig. 16, panel A) representing about 3 cm of LoS displacement (Fig. 16, panel B).

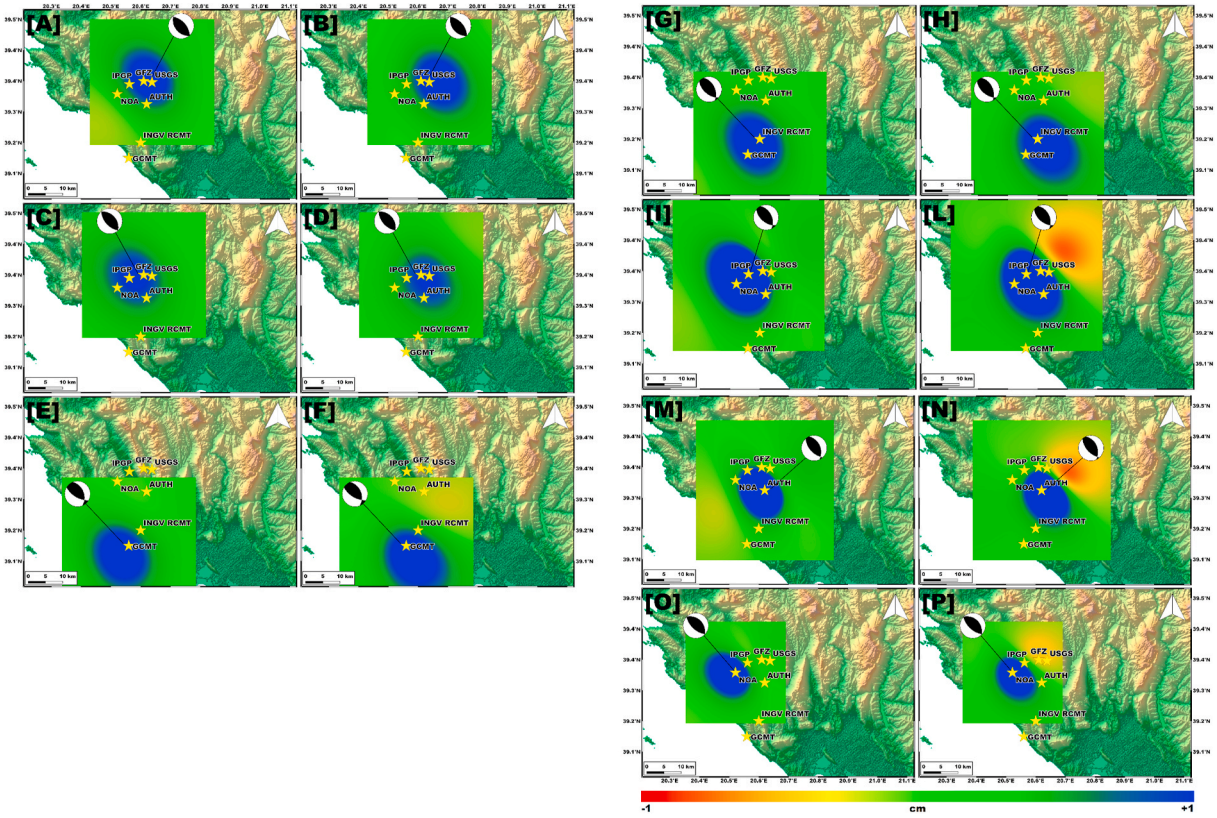

Fig. 15. LoS coseismic ground displacement of the 2021 Grecia earthquake simulated from USGS (A,B), GFZ (C,D), GCMT (E,F) INGV RCMT (G,H), IPGP (I,L), AUTH (M,N) and NOA (O,P) moment tensor solutions and projected along S1 ascending (left column) and descending (right column) track. The yellow stars indicate the epicenters estimated by the agencies. The background image is the SRTM DEM. (For interpretation of the references to colour in this figure legend, the reader is referred to the Web version of this article.)

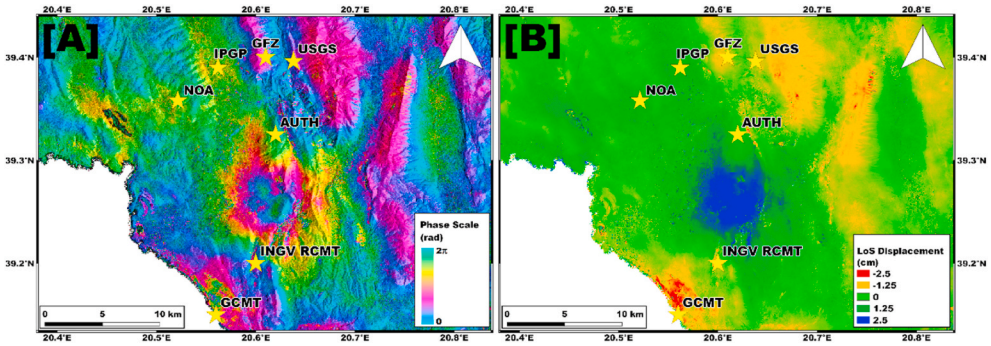

Fig. 16. S1 Wrapped interferogram (A) and Displacement map (B) related to the 2020 Greece earthquake.

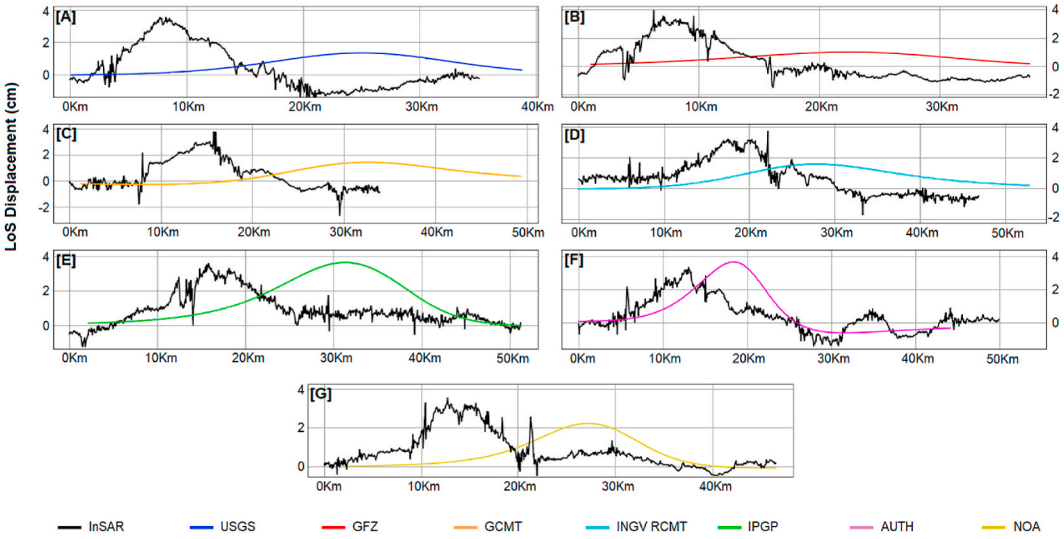

Fig. 17. Comparison between LoS displacement retrieved by InSAR data and derived from USGS [A], GFZ [B], GCMT [C], INGV RCMT [D], IPGP [E], AUTH [F] and NOA [G] solutions along transepts crossing the related peak deformation values in the case of 2020 Greece earthquake.

InSAR ground deformation pattern is in satisfying agreement with the ones simulated meaning that the fault geometry is quite well constrained by all the solutions and a profile analysis is needed. Then, we analyse several profiles crossing the maximum deformation values to evaluate the peak-to-peak distance between estimated (from InSAR data) and simulated (from moment tensors) seismic-induced displacement fields (see Fig. 17).

The best solution in terms of location and magnitude is the one retrieved from AUTH moment tensor solution which quite well reproduces the real seismic-induced deformation estimated by InSAR data. There is a slight shift of about 4–5 Km between the two solutions but the kinematics estimated from AUTH is very close to the one retrieved by inversion of InSAR data as shown in Svikgas et al. (2021).

IPGP and NOA solutions are consistent in magnitude likely meaning that the kinematics is close to the real case but not in location showing a peak-to-peak distance of about 15 Km and 12 Km, respectively. INGV RCMT solution underestimates the real deformation but the location is far about 7 Km. USGS, GFZ and GCMT solutions significantly underestimate the deformation probably due to a deeper causative fault with respect to the real and also fail about the location showing tens of km between estimated and simulated deformation peaks.

5.7. Croatia

This event occurred a few Km north of Zagabria city, close to the boundaries between Croatia and Slovenia. Four moment tensor solutions were provided by USGS, GFZ, INGV TDMT and INGV RCMT. They show a quasi pure reverse faulting mechanism except for the INGV RCMT solution due to a rake angle quite different from 90°. This involves a different sensitivity to the two satellite geometry of view returning in a more pronounced simulated displacement field when projected along descending orbit (Fig. 18, panel G,H). On the other hand, USGS, GFZ and INGV TDMT solutions do not show significant differences between ascending and descending orbit, then we chose S1 descending data for performing the InSAR analysis.

We selected the pair acquired on March 22nd and 28th, 2020 to image the coseismic displacement by InSAR processing obtaining the results shown in Fig. 19. We detected one interferometric fringe representing a LoS Displacement of about 3 cm (Fig. 19, panel A,B). Also in this case, the real deformation pattern is in agreement with the ones simulated by USGS, GFZ, INGV TDMT and RCMT solutions thus we further evaluate the consistency by profile analysis (Fig. 20). All the solutions underestimate of about 2 cm the real deformation, in this sense

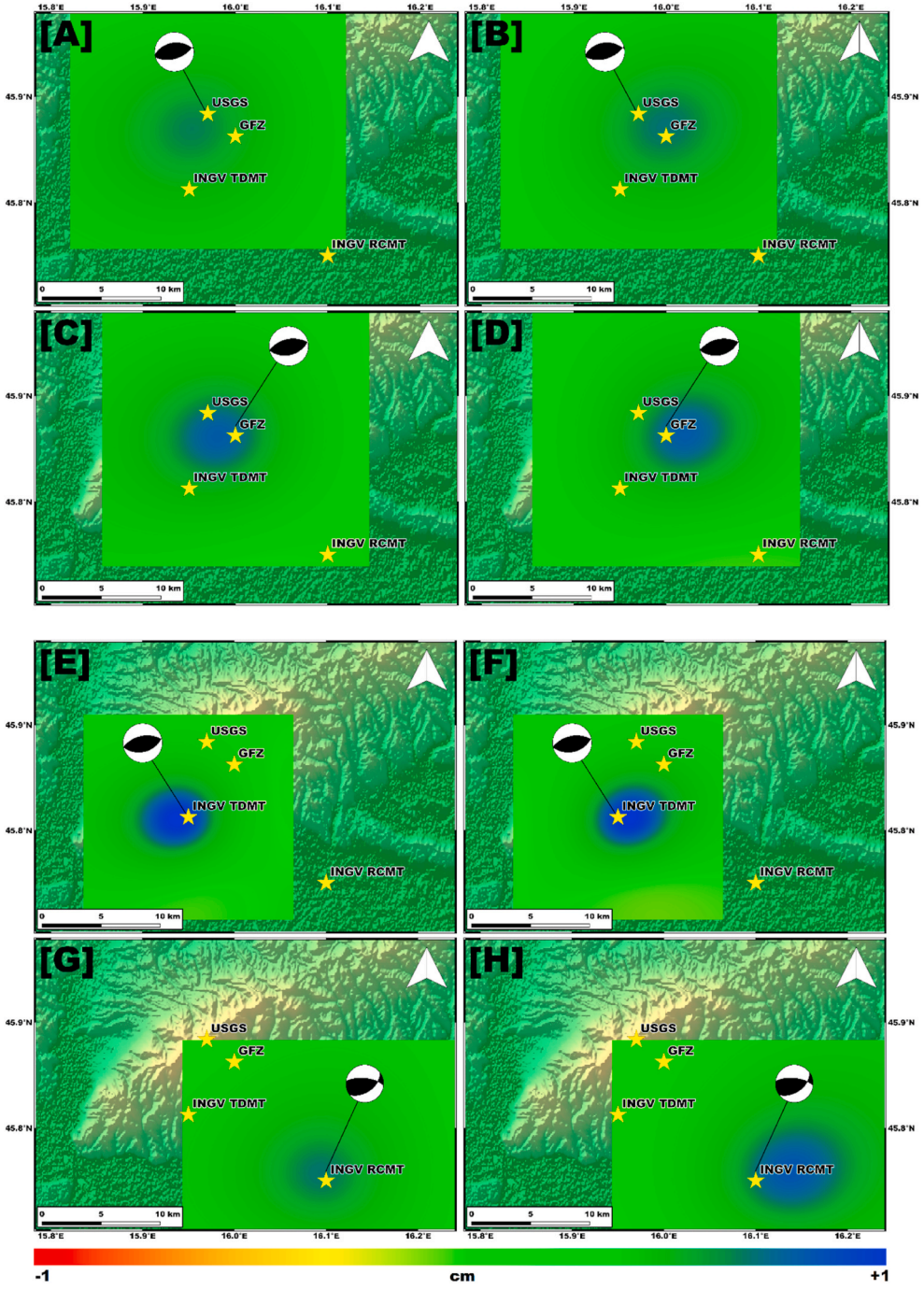

Fig. 18. LoS coseismic ground displacement of the 2021 Grecia earthquake simulated from USGS (A,B), GFZ (C,D), INGV TDMT (E, F) and INGV RCMT (G,H) moment tensor solutions and projected along S1 ascending (left column) and descending (right column) track. The yellow stars indicate the epicenters estimated by the agencies. The background image is the SRTM DEM. (For interpretation of the references to colour in this figure legend, the reader is referred to the Web version of this article.)

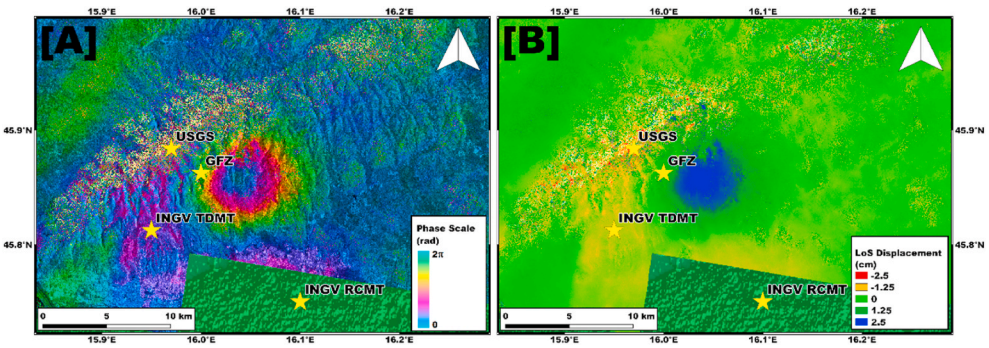

Fig. 19. S1 Wrapped interferogram (A) and Displacement map (B) related to the 2020 Croatia earthquake.

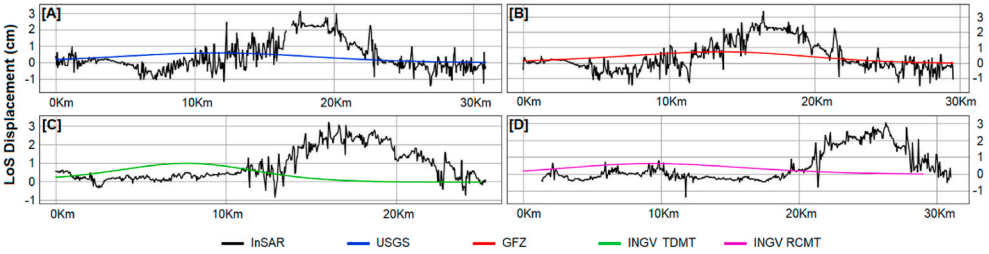

Fig. 20. Comparison between LoS displacement retrieved by InSAR data and derived from USGS [A], GFZ [B], INGV TDMT [C] and INGV RCMT [D] solutions along transepts crossing the related peak deformation values in the case of 2020 Croatia earthquake.

the best solution is the one provided by INGV TDMT peaking just over 1 cm consistently with a shallower source found at 6 km with respect to the other solutions (see Table 2). Conversely, the GFZ solution is the closest to the real epicenter showing a peak-to-peak distance of about 2.5 Km.

6. Discussion

The proposed procedure has been adopted for studying several seismic events including both mainly normal/reverse and strike-slip faulting mechanisms to provide a synoptic view of the performances (see Tables 3 and 4). The aim is to evaluate the variability of the solutions provided by the agencies in case of light-to-moderate earthquakes, i.e. when constraining location and kinematics of an event is quite hard. Indeed, in these cases, the solutions often differ greatly from each other and here we want to understand which are the most important parameters leading this process and the best solutions according to the developed procedure.

In particular, we tested the procedure on one normal faulting mechanism event, i.e. the Turkey earthquake, four reverse or quasi-reverse faulting mechanism events, i.e. the Algeria, France, Greece and Croatia earthquakes, and two strike-slip faulting mechanism events, i.e. the Bosnia-Herzegovina and Italy earthquakes.

However, general outcomes connected to the faulting mechanism of the seismic events are hard to be retrieved since the results both in terms of predicted scenarios and InSAR-derived coseismic deformation show a

Table 3
Table of the distance between the peaks of the simulated and estimated coseismic displacement field. SNA stands for *Solution Not Available* whereas NE indicates *Not Estimated* since the predicted scenarios don't show any deformation pattern.

	USGS	GFZ	GCMT	KOERI	ERD	INGV RCMT	INGV TDMT	IPGP	AUTH	NOA
Algery	10 Km	7 Km	SNA	SNA	SNA	6 km	SNA	SNA	SNA	SNA
Italy	3.5 Km	SNA	SNA	SNA	SNA	NE	1.5 Km	SNA	SNA	SNA
Turkey	9 Km	4 Km	8 Km	2 Km	0.5 Km	SNA	SNA	20 Km	SNA	SNA
France	NE	NE	SNA	SNA	SNA	NE	SNA	SNA	SNA	SNA
Bosnia	NE	NE	SNA	SNA	SNA	NE	NE	SNA	SNA	SNA
Croatia	5 km	3 km	SNA	SNA	SNA	16 km	9 Km	SNA	SNA	SNA
Greece	16 Km	13 Km	17 Km	SNA	SNA	7.5 Km	SNA	15 Km	4.5 Km	12 Km

Table 4
Table of the difference of intensity between the peaks of the simulated and estimated coseismic displacement field. SNA stands for *Solution Not Available* whereas NE indicates *Not Estimated* since the predicted scenarios don't show any deformation pattern.

	USGS	GFZ	GCMT	KOERI	ERD	INGV RCMT	INGV TDMT	IPGP	AUTH	NOA
Algery	8 cm	9 cm	SNA	SNA	SNA	8 cm	SNA	SNA	SNA	SNA
Italy	11 cm	SNA	SNA	SNA	SNA	NE	13 cm	SNA	SNA	SNA
Turkey	3 cm	3 cm	0.5 cm	2.2 cm	3 cm	SNA	SNA	0.5 cm	SNA	SNA
France	NE	NE	SNA	SNA	SNA	NE	SNA	SNA	SNA	SNA
Bosnia	NE	NE	SNA	SNA	SNA	NE	NE	SNA	SNA	SNA
Croatia	2.1 cm	2 cm	SNA	SNA	SNA	1.7 cm	2 cm	SNA	SNA	SNA
Greece	1.7 cm	2.5 cm	1.6 cm	SNA	SNA	1.6 cm	SNA	0.2 cm	0.1 cm	1.3 cm

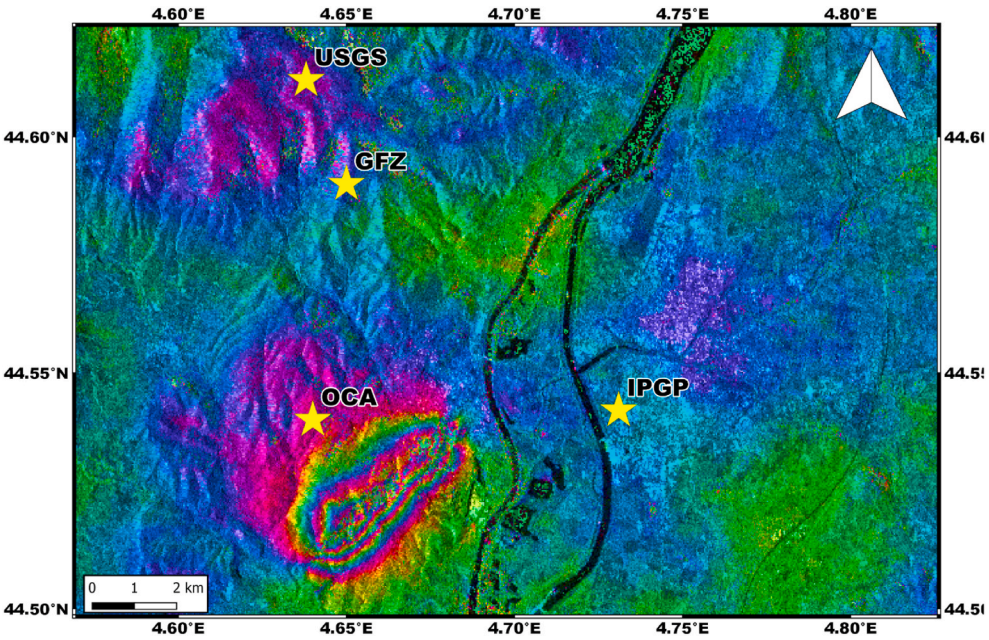

Fig. 21. Focus on the epicenter locations estimated by IPGP and OCA in the case of France earthquake.

great variability.

Indeed, the last step of the procedure, which theoretically indicates the best conditions, when there is a good agreement between predicted and real scenario, is reached only for four events spanning between all the different mechanisms, i.e. Italy, Turkey, Greece and Croatia earthquakes, representing just over 50% of the considered dataset.

Instead, the best performance of the procedure seems to be more connected to the magnitude and the depth of the seismic event. In particular, best results are retrieved as the larger the magnitude and/or the shallower the depth of the earthquake. Indeed, as shown in Table 2, Turkey and Greece earthquake are characterized by the largest magnitude of the dataset (about Mw 5.7 estimated by all agencies) whereas the Italy earthquake is the shallower one (1 Km and 3 Km for the USGS and INGV TDMT solutions, respectively).

This is quite expected since the propagation of the seismic energy along the surface is strictly connected to these two parameters. As larger is the magnitude and/or shallower the depth of the seismic source then the coseismic surface displacement field will probably be more pronounced. Accordingly, when we deal with strong and clear coseismic displacement fields (because of the higher magnitude or the shallow depth) it is reasonable to expect a good agreement between the different solutions and between predicted and real scenarios.

The depth of the seismic source plays an important role also for Bosnia-Herzegovina and France case studies. Bosnia-Herzegovina is the only test case where both predicted and real scenarios don't show any surface deformation pattern. This is due to the significant depth spanning from 10 to 32 Km estimated by all the agencies which most likely agrees with the real depth thus not allowing the seismic waves to propagate till the surface.

Also for the France earthquake no signals are observed in predicted scenarios, theoretically meaning that the depth estimated by the solutions (about 10 Km), together with the light magnitude of the event (Mw 4.8–4.9), prevent the propagation of any signals to the surface. However, in this case, the real InSAR-derived scenario significantly differs showing a clear deformation pattern peaking at about -+3 cm. As a matter of fact, the estimated depths are not consistent with those real, being the France earthquake a very shallow seismic event as shown in literature (Cornou et al., 2021; Causse et al., 2021).

Particular care is instead required for analyzing the results of Croatia and Algeria earthquakes. In the first case, the procedure was entirely performed and we found the best agreement between the predicted scenario from GFZ and INGV TDMT solutions. In particular, GFZ solution is the most accurate in terms of position of the deformation pattern (about 3 Km far from the real) whereas INGV TDMT is the best reproducing the intensity of the coseismic deformation being the estimated seismic source depth the shallower between all the agencies solutions (about 6 Km depth). Conversely, despite the similar magnitude, depth and focal mechanism, in the second case, the procedure ends before the last step since predicted and real scenarios are inconsistent. Such discrepancy is most likely due to the different density of the seismic networks used for estimating the solutions of such two events and also the azimuthal coverage in Algeria is probably not optimal.

It is interesting to note how for Italy, Turkey and Greece earthquakes the best solutions in terms of epicenter location are provided by national institutions or authorities, i.e. the Italian INGV TDMT for Italy case study, the Turkish ERD for Turkey case study and the Greece AUTH for Greece case study. Indeed, most of agencies exploit regional velocity models in the analysis of seismic events occurred within their national boundaries (Herrmann et al., 2011). The use of an appropriate regional velocity model is important to define the moment magnitude of the earthquake because the theoretical amplitudes at high frequencies depend very strongly on the velocity model. In case of light to moderate events, they are more reliable and accurate than global crustal models as the PREM (Preliminary Reference Earth Model, Dziewonski and Anderson, 1981), used for example by INGV RCMT worldwide, that can instead may be suitable for greater magnitude across the Mediterranean region (periods longer than 100 s, Mw $>$ 6). In addition, in some cases the national seismic networks are integrated by temporary stations to improve the density and the azimuthal coverage and refine the estimation of source parameters.

Also for the France earthquake, the epicenter locations estimated by two french agencies, i.e. IPGP and OCA are the closest to the real deformation (Fig. 21). However, the procedure is not applicable for the solution provided by such agencies since they do not provide the seismic moment which is needed to simulate the coseismic deformation.

7. Conclusion

In this work we proposed a procedure based on satellite InSAR data to analyse the variability of the moment tensor solutions estimated by

several agencies in case of light-to-moderate earthquakes. We focused on a dataset consisting of seven seismic events that occurred in the Mediterranean area, but the procedure can be easily extended worldwide to study any seismic event occurred inland. Thanks to the different peculiarities of the events, the selected dataset allows to evaluate the performance of the procedure in several case studies covering reverse, normal and strike-slip faulting mechanism. We found some correlation between the precision of the solutions and the main parameters of the seismic source, such as magnitude and depth whereas the focal mechanism seems not to play an important role in this context. Moreover, the adopted velocity model and the distribution of the seismic stations used by the different agencies for constraining the seismic source have also to be taken into account to evaluate the variability of the solutions since regional models show better results than global ones.

The proposed procedure show how for light-to-moderate earthquakes there is a great variability of the solutions depending on several factors both intrinsically related to the seismic event such as depth and magnitude and connected to the estimated solution as the density of seismic network, the adopted velocity model and the azimuth coverage.

Declaration of competing interest

The authors declare that they have no known competing financial interests or personal relationships that could have appeared to influence the work reported in this paper.

Acknowledgements

The authors thank the European Space Agency for providing C-band Sentinel-1 SAR data used in this work. In addition, the authors thank all the INGV GeoSAR Laboratory working group for the useful suggestions exploited for improving the present research article.

References

Albano, M., Saroli, M., Montuori, A., Bignami, C., Tolomei, C., Polcari, M., Pezzo, G., Moro, M., Atzori, S., Stramondo, S., Salvi, S., 2018. The relationship between InSAR coseismic deformation and earthquake-induced Landslides Associated with the 2017 Mw 3.9 Ischia (Italy) earthquake. Geosciences 8, 303. https://doi.org/10.3390/geosciences8080303.

Atzori, S., Hunstad, I., Chini, M., Salvi, S., Tolomei, C., Bignami, C., Stramondo, S., Trasatti, E., Antonioli, A., Boschi, E., 2009. Finite fault inversion of DInSAR coseismic displacement of the 2009 'Aquila earthquake (Central Italy). Geophys. Res. Lett. 36 https://doi.org/10.1029/2009GL039293.

Azzaro, R., Mattia, M., Puglisi, G., 2001. Fault creep and kinematics of the eastern segment of the Pernicana Fault (Mt. Etna, Italy) derived from geodetic observations and their tectonic significance. Tectonophysics 333 (3–4), 401–415. https://doi.org/10.1016/S0040-1951(01)00021-X.

Bonforte, Alessandro, Guglielmino, Francesco, Puglisi, Giuseppe, 2019. Large dyke intrusion and small eruption: the December 24, 2018 Mt. Etna eruption imaged by Sentinel-1 data, 31. Terra Nova, pp. 405–412. https://doi.org/10.1111/ter.12403.

Causse, M., Cornou, C., Maufroy, E., et al., 2021. Exceptional ground motion during the shallow Mw 4.9 2019 Le Teil earthquake, France. Commun Earth Environ 2, 14. https://doi.org/10.1038/s43247-020-00089-0.

Cheloni, D., et al., 2017. Geodetic model of the 2016 Central Italy earthquake sequence inferred from InSAR and GPS data. Geophys. Res. Lett. 44 https://doi.org/10.1002/2017GL073580.

Cornou, Cécile, et al., 2021. Rapid response to the M_w 4.9 earthquake of November 11, 2019 in Le Teil, lower Rhône Valley, France. In: Comptes Rendus. Géoscience, Online first, pp. 1–23. https://doi.org/10.5802/crgeos.30.

Costantini, M., 1998. A novel phase unwrapping method based on network programming. IEEE Trans. Geosci. Rem. Sens. 36, 813–821.

De Novellis, V., Atzori, S., De Luca, C., Manzo, M., Valerio, E., Bonano, M., Cardaci, C., Castaldo, R., Di Bucci, D., Manunta, M., Onorato, G., Pepe, S., Solaro, G., Tizzani, P., Zinno, I., Neri, M., Lanari, R., Casu, F., 2019. DInSAR analysis and analytical modeling of Mount Etna displacements: the december 2018 Volcano-tectonic Crisis. Geophys. Res. Lett. 46, 5817–5827. https://doi.org/10.1029/2019GL082467.

Dziewonski, A.M., Chou, T.-A., Woodhouse, J.H., 1981. Determination of earthquake source parameters from waveform data for studies of global and regional seismicity. J. Geophys. Res. 86, 2825–2852. https://doi.org/10.1029/JB086iB04p02825.

Goldstein, R., Werner, C., 1998. Radar interferogram filtering for geophysical applications. Geophys. Res. Lett. 25, 4035–4038.

Herrmann, R.B., Malagnini, L., Munafò, I., 2011. Regional moment tensor of the 2009 L'Aquila earthquake sequence. Bull. Seismol. Soc. Am. 101 (3), 975–993. https://doi.org/10.1785/0120100184.

Karasözen, E., Karasözen, B., 2020. Earthquake location methods. Int. J. Geom. 11, 13. https://doi.org/10.1007/s13137-020-00149-9.

Kobayashi, T., Tobita, M., Koarai, M., et al., 2012. InSAR-derived crustal deformation and fault models of normal faulting earthquake (Mj 7.0) in the Fukushima-Hamadori area. Earth Planets Space 64, 15. https://doi.org/10.5047/eps.2012.08.015.

Lentas, K., Di Giacomo, D., Harris, J., Storchak, D.A., 2019. The ISC Bulletin as a comprehensive source of earthquake source mechanisms. Earth Syst. Sci. Data 11, 565–578. https://doi.org/10.5194/essd-11-565-2019.

Massonnet, Didier, Feigl, Kurt L., 1998. Radar interferometry and its application to changes in the Earth's surface. Reviews of Geopsysics 36, 441–500. https://doi.org/10.1029/97RG03139.

Massonnet, D., Rossi, M., Carmona, C., et al., 1993. The displacement field of the Landers earthquake mapped by radar interferometry. Nature 364, 138–142. https://doi.org/10.1038/364138a0.

Neri, M., Acocella, V., Behncke, B., 2004. The role of the Pernicana Fault System in the spreading of Mt. Etna (Italy) during the 2002–2003 eruption. Bull. Volcanol. 66, 417–430. https://doi.org/10.1007/s00445-003-0322-x.

Okada, Yoshimitsu, 1985. Surface deformation due to shear and tensile faults in a half-space. Bull. Seismol. Soc. Am. 75 (4), 1135–1154. https://doi.org/10.1785/BSSA0750041135.

Pondrelli, S., 2002. European-mediterranean Regional Centroid-Moment Tensors Catalog (RCMT) [Data Set]. Istituto Nazionale di Geofisica e Vulcanologia. https://doi.org/10.13127/rcmt/euromed (INGV).

Schmidt, D.A., Bürgmann, R., 2006. InSAR constraints on the source parameters of the 2001 Bhuj earthquake. Geophys. Res. Lett. 33 (2) https://doi.org/10.1029/2005GL025109.

Scognamiglio, L., Tinti, E., Quintiliani, M., 2006. Time Domain Moment Tensor (TDMT) [Data Set]. Istituto Nazionale di Geofisica e Vulcanologia. https://doi.org/10.13127/TDMT (INGV).

Svigkas, N., Kiratzi, A., Antonioli, A., Atzori, S., Tolomei, C., Salvi, S., Polcari, M., Bignami, C., 2021. Earthquake source investigation of the Kanallaki, March 2020 sequence (North-Western Greece) based on seismic and geodetic data. Rem. Sens. 13, 1752. https://doi.org/10.3390/rs13091752.

Wang, L., Gao, H., Feng, G., Xu, W., 2018. Source parameters and triggering links of the earthquake sequence in central Italy from 2009 to 2016 analyzed with GPS and InSAR data. Tectonophysics 744, 285–295.

Wang, L., Zhao, X., Xu, W., Xie, L., Fang, N., 2019. Coseismic slip distribution inversion with unequal weighted Laplacian smoothness constraints. Geophys. J. Int. 218 (1), 145–162.

Wells, Donald L., Coppersmith, Kevin J., 1994. New empirical relationships among magnitude, rupture length, rupture width, rupture area, and surface displacement. Bull. Seismol. Soc. Am. 84 (4), 974–1002.

Wright, Tim J., Lu, Zhong, Chuck Wicks, 2003. Source model for the Mw 6.7, 23 October 2002, Nenana Mountain earthquake (Alaska) from InSAR. Geophys. Res. Lett. 30 (18) https://doi.org/10.1029/2003GL018014.